Smart Structures and Systems, *Vol. 34, No. 1 (2024) 33-40*
https://doi.org/10.12989/sss.2024.34.1.033

Embedded type new in-situ soil stiffness assessment and monitoring technique

Namsun Kim [1a], Jong-Sub Lee [1b], Younggeun Yoo [1c], Jinwook Kim [1c] and Junghee Park*[2]

[1] *School of Civil, Environmental and Architectural Engineering, Korea University, 145, Anam-ro, Seongbuk-gu, Seoul, 02841, Republic of Korea*
[2] *Department of Civil and Environmental Engineering, Incheon National University, 119 Academy-ro, Yeonsu-gu, Incheon 22012, Republic of Korea*

(*Received May 15, 2024, Revised August 17, 2024, Accepted August 20, 2024*)

Abstract. We aimed to assess the evolution of small-strain stiffness and relative density in non-compacted embankment layers. We developed embedded type in-situ soil stiffness measurement devices for monitoring small-strain stiffness occurring after filling at a test site and conducted comprehensive laboratory compaction tests using an oedometer cell with a bender element. However, direct comparison is extremely difficult because the shear wave velocity measured in the field and laboratory depend on depth and effective stress, respectively. Therefore, we propose a method for establishing a relationship between effective stress and depth using a compressibility model. In this study, the shear wave velocity measured in the field was compared to the estimated shear wave velocity-depth profiles for completely dry and saturated conditions with different relative densities. The relative density under saturated soil conditions may vary between 50% and 90% and tends to be closer to 95%. Under dry soil conditions, the relative density of the embankment can vary from 30% to 70% and tends to approach 76%. For model validation, the relative density estimated from shear wave velocity-depth profiles was compared to that estimated from DCPI data. In other words, the results analyzed in the context of an effective stress–depth model enable the prediction of engineering properties such as the small-strain stiffness and relative density of embankment layers. This study demonstrates that physics-based data analyses successfully capture the relative density of non-compacted embankment layers.

Keywords: compressibility model; embedded type in-situ soil stiffness measurement device; non-compacted embankment layer; relative density; small-strain stiffness

1. Introduction

The relative density of an embankment layer with coarse-grained soil is critical for various engineering and construction projects. These physical properties directly influence the stability, strength, stiffness, and performance of structures built on embankment layers (Kim *et al*. 2001, He *et al*. 2020, Spagnoli and Shimobe 2020, Ifediniru and Ekeocha 2022). In this context, in-situ density testing, such as the sand cone test, is critical for determining soil compaction and relative density in the field. However, despite being commonly used, doubts remain regarding the accuracy and reliability of field-density testing techniques. Therefore, a suitable investigative approach is required to assess geotechnical engineering properties to ensure the stability of the embankment layer.

In geotechnical engineering, relative density commonly denotes the level of compaction observed in coarse-grained soils. This parameter indicates the relative placement of the field void ratio e within the spectrum bounded by the maximum e_{max} and minimum e_{min} void ratios (Chang *et al*. 2006, Chian *et al*. 2017). However, practical issues exist, such as the determination of the void ratio, particularly in solid-volume measurements. Thus, the relative density is primarily expressed in terms of the dry density because of the inherent difficulty of directly measuring the void ratio. The sand cone test is recognized as the most widely used method for measuring field density. However, because the sand cone test is conducted at specific locations (i.e., spot tests), it presents limitations in real-time and continuous quality management of the entire site based solely on these results (Choi *et al*. 2021). Alternatively, empirical approaches have been proposed to assess the relative density of sandy soils using in-situ tests, such as the dynamic cone penetration test DCPT (Mohammadi *et al*. 2008, MacRobert *et al*. 2019, Kim *et al*. 2021). However, the strength properties of soils, such as the DCPI, inherently harbor uncertainties owing to the variability in ground composition (e.g., presence of stones or gravel); hence, proficient technicians and meticulous analyses are indispensable (Park *et al*. 2022).

The seismic design of an embankment layer at a construction site typically depends on specific engineering properties and state parameters. Accurately estimating the stress-dependent shear wave velocity of soils is critical for analyzing the dynamic ground response, seismic soil-structure interactions, and soil liquefaction potential in

*Corresponding author, Ph.D., Assistant Professor,
E-mail: junghee.park@inu.ac.kr
[a] Ph.D., E-mail: Postdoctoral Researcher
[b] Ph.D., Professor
[c] Ph.D. Student

ISSN: 1738-1584 (Print), 1738-1991 (Online)

geotechnical engineering studies (Andrus and Stokoe 2000, NEHRP 2003, Byun *et al*. 2015, Naing *et al*. 2015, Ji *et al*. 2021). Conventional shear wave velocity profiling methods, seismic refraction surveys, crosshole seismic tests, downhole seismic tests, surface wave methods, and borehole shear wave logging have been used to design geotechnical structures safely. However, variations in shear wave velocity among survey methods can be attributed to several factors: (1) differences in the scale of the medium, (2) errors that occur during data analysis, and (3) different wave propagation characteristics (Stewart and Campanella 1993, Brown *et al*. 2002). In this context, new measurement and analysis techniques are required to accurately investigate design parameters.

This study aims to evaluate the relative density and small-strain stiffness of noncompacted embankment layers using a nondestructive approach. First, we introduced an embedded-type in-situ soil stiffness measurement device for the evaluation of small-strain stiffness by measuring the elastic waves in the embankment layer. Next, we discuss field and laboratory experimental results. Next, we attempted to establish a relationship between the effective stress and depth using a compressibility model and laboratory results. This closed-form solution provides geotechnical properties, such as the relative density with depth in noncompacted embankment layers. Finally, to validate the model, we compared the relative densities estimated from the DCPI data with those calculated using the relative density-depth model.

2. Site description

Fig. 1(a) shows the test bed with dimensions of 80 × 100 × 5 m (width × length × height). To preserve the non-compacted conditions, fill material was deposited on the surface without compaction, followed by leveling. A field test was performed at the midpoint of the embankment site to exclude potential impacts from the landfill slope. The embankment construction involved layers of 0.5, 1.5, 3.5, 4.5, and 5 m with embedded type in-situ soil stiffness measurement devices installed for each layer.

Fig. 1(b) shows the particle size distribution curve of the fill materials obtained from the test site. According to the Unified Soil Classification System (USCS), the soil is categorized as well-graded sand (SW). The index properties of the fill material are as follows: specific gravity (G_s) = 2.65, coefficient of uniformity (C_u) = 6.69, and coefficient of curvature (C_c) = 1.18. Furthermore, the soil water content in the field was less than 7%, indicating dry conditions.

3. Experimental study

3.1 Embedded type in-situ soil stiffness measurement device

An embedded type in-situ soil stiffness measurement device was developed to monitor seismic waves in a non-compacted embankment during each filling stage. Fig. 2(a) illustrates a schematic of the newly designed device. This device adopted the shape of a box with dimensions of 200 × 50 × 50 mm (width × length × height). To safeguard the sensor and ensure long-term functionality, three pairs of bender elements (BEs) are positioned within the front groove.

The bender element was 15 mm in length and 10 mm in width. Bender elements (BEs) were first coated with a thin layer of epoxy, and then painted with a conductive layer to serve as an electrical shield. Finally, they were encased in another thin layer of epoxy for waterproofing, while preserving their vibration characteristics (Lee and Santamarina 2005). Bender elements (BEs) were positioned within a threaded nylon tube and inserted vertically into box-shaped frames. The parallel-type bender element used in this study was composed of a conductive thin metal shim, two layers of piezoceramic plate, and two conductive outer electrodes. When subjected to an electric field, piezoceramic plates undergo mechanical deformation and generate an electrical charge, enabling the conversion between electrical and physical signals. Consequently, BEs can serve as both sources and receivers of shear waves by generating and detecting them using piezoelectricity. In addition, the distance between the source and receiver BEs can be adjusted. In this study, the tip-to-tip distance was set to 250 mm because of the attenuation of the amplitude and the clear detection of the time to the first arrival of the shear wave signatures.

Fig. 3 shows the measurement system of the measurement device. To propagate waves through the medium, a signal generator supplies input signals, such as square waves or single sine waves, with amplitudes of up to

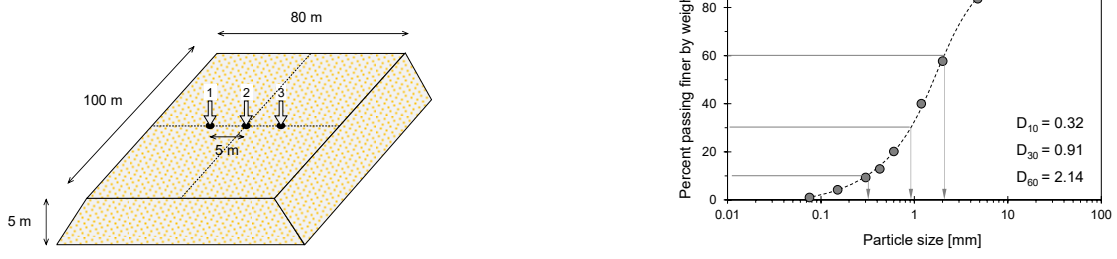

(a) Testbed (b) Particle size distribution for embankment materials

Fig. 1 Non-compacted embankment testbed description

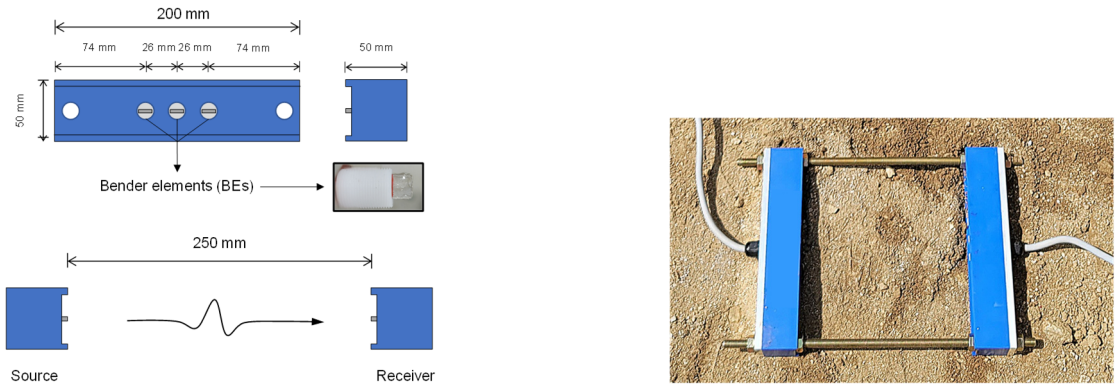

(a) Schematic drawing (b) Picture

Fig. 2 Embedded type in-situ soil stiffness measurement device

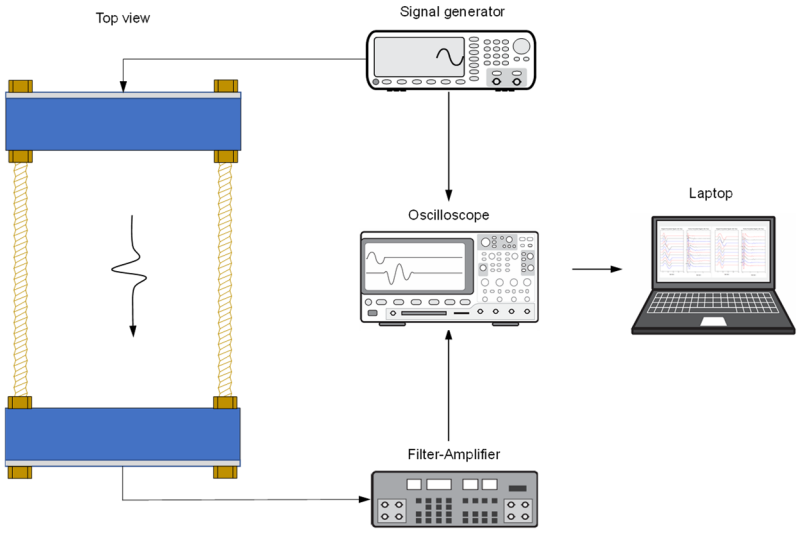

Fig. 3 Measurement system of embedded type in-situ soil stiffness measurement device

10 volts to both the source and oscilloscope. The receiver captured the output signal that propagated through the medium. Subsequently, the filtered and amplified output signals were visualized using an oscilloscope after passing through a filter amplifier.

3.2 Oedometer cell instrumented with BEs

A standard oedometer test assesses the load-deformation behavior of a specimen. However, for a comprehensive comparison of the field measurement results, shear wave velocity analysis in terms of the vertical effective stress is required. Therefore, in this study, oedometer cells equipped with BEs were used to determine the small–strain stiffness of the specimens at different loading steps. Fig. 4 shows a schematic drawing and measurement system for the newly designed oedometer cell. The oedometer cell comprised a thick nylon cell with a diameter of 98.8 mm and a wall thickness of 25 mm, within which the specimen was positioned. A pair of bender elements was installed in the top and bottom caps to measure the shear wave.

In the laboratory tests, the soil specimens were compacted to achieve the specified densities (e.g., D_r = 30, 50, 70, and 90%). During each loading and unloading step,

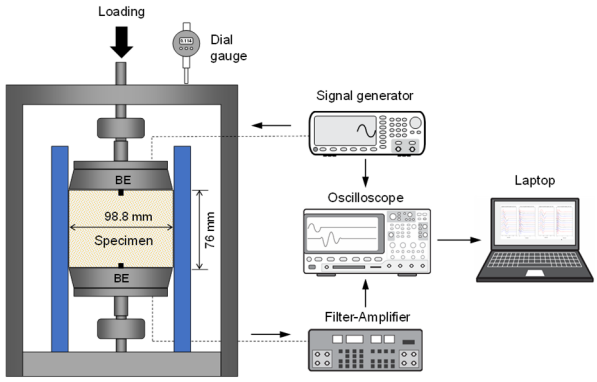

Fig. 4 Schematic drawing and measurement system of oedometer cell instrumented with bender elements

vertical stresses of 5, 10, 30, 60, 125, 250, and 500 kPa were applied, respectively. The applied stresses, shear wave velocities, and deformations were monitored using load cells, bender elements (BEs), and digital gauges. The wave measurement system was equivalent to a device used in the field, as described previously.

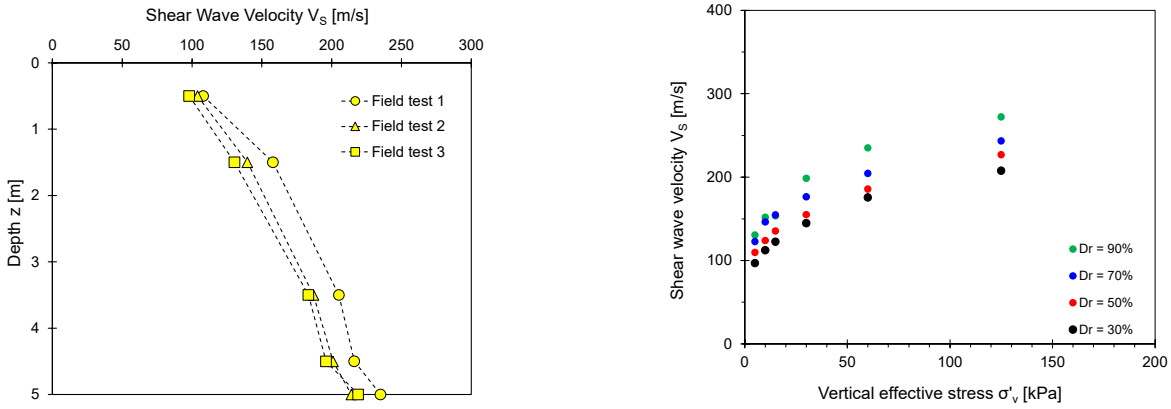

(a) Shear wave velocity obtained from field tests (b) Shear wave velocity obtained from laboratory tests

Fig. 5 Shear wave velocity

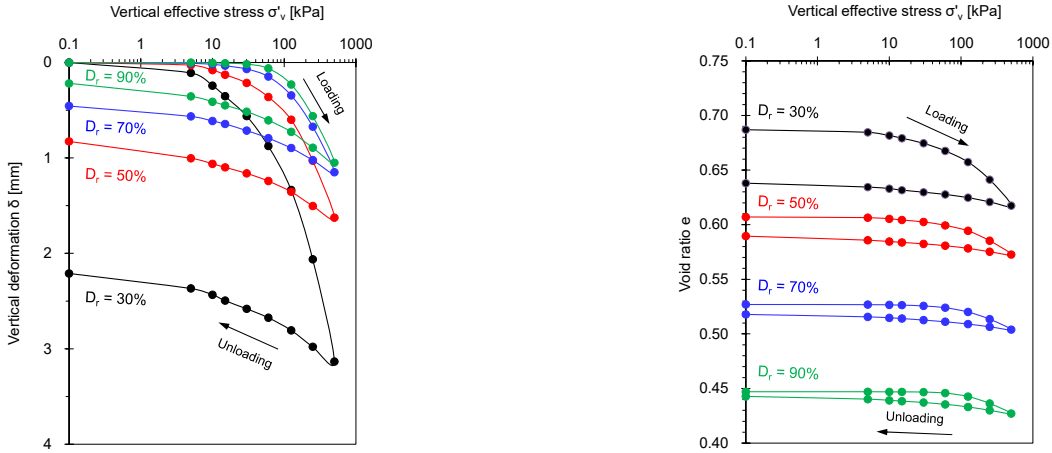

(a) Deformation (b) Void ratio

Fig. 6 Oedometer test results

4. Experimental results

4.1 Shear wave velocity

The characterization of soils using shear waves relies on microscale behavior, which entails minor disturbances within granular media without altering its structure. In other words, this reaction is subject to stress and inherent fabric characteristics, as determined by the velocity of wave propagation or stiffness under small strains (Hoang *et al.* 2022). In this context, the shear wave velocity propagating through the soil can be determined by measuring the distance between the source and receiver bender elements (L) and the travel time of the shear wave (t)

$$V_S = \frac{L}{\Delta t} \tag{1}$$

Fig. 5 presents both field and laboratory experimental results related to effective stress-dependent geotechnical properties such as shear wave velocity. The shear wave velocity measured at each stage of filling of the embankment layer is shown in Fig. 5(a). The results indicated that the shear wave velocity, as measured by an in-situ soil stiffness measurement device buried at equivalent depths within the embankment layer, exhibited a consistent trend and gradually increased as the depth increased. Fig. 5(b) plots the shear wave velocity in terms of the vertical effective stress, as measured for specimens with four distinct relative densities (D_r = 30%, 50%, 70%, and 90%) during laboratory tests.

4.2 Load–deformation behavior

Fig. 6(a) presents the deformation results of the dry specimens under varying effective stress conditions observed during the loading and unloading laboratory tests. These results were used to calculate the void ratio, as shown in Fig. 6(b). The results indicated that the void ratio of all the specimens in the initial state decreased steadily as the vertical effective stress increased. Notably, the void ratio exhibited a relatively significant increase when the effective stress increased from 250 to 500 kPa. Furthermore, volume reduction became more pronounced as the relative density decreased.

Table 1 Constitutive parameters for compressibility model and shear wave factors for four specimens with D_r = 30, 50, 70, and 90% (Exponential model η = 0.33)

Relative density D_r [%]	Compressibility model parameter			Shear wave factors	
	e_L	e_H	σ'_c [kPa]	α [m/s]	β
30	0.715	0.455	5500	63.70	0.250
50	0.625	0.480	6000	69.10	0.249
70	0.540	0.440	7000	75.40	0.247
90	0.460	0.350	15000	86.60	0.240

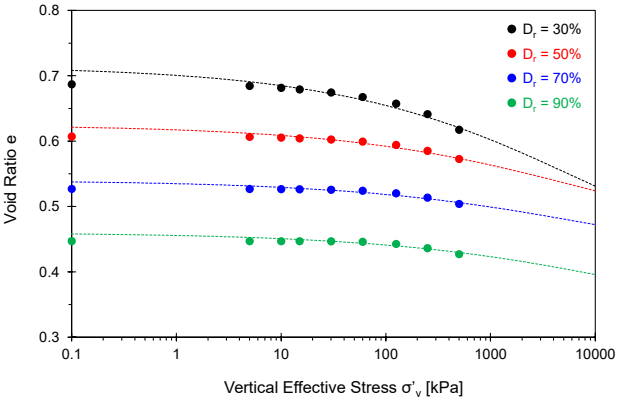

Fig. 7 Compression curves with a wide stress range based on soil compressibility model

5. Analyses and discussion

5.1 Soil compressibility model – Effective stress versus void ratio

The Terzaghi model can be expressed as a function of the void ratio and vertical effective stress as follows: $e = e_o - C_c \cdot \log(\sigma'/\sigma'_o)$ (Terzaghi *et al*. 1996). The compaction trend based on this model shows a linear volumetric behavior of cohesionless soils in one-dimensional compression; thus, the Terzaghi model does not meet exponential conditions under very low and high effective stresses owing to the nonlinear compaction trend (Burland 1990, Pestana and Whittle 1955). In this study, we used an exponential soil compressibility model that reflects the void ratio e_L at low effective stresses and e_H at very high effective stresses (Chong and Santamarina 2016, Lyu *et al*. 2021, Kim *et al*. 2024). The void ratio e_z at a given depth is subsequently determined as a function of the vertical effective stress σ'_z

$$e_z = e_H + (e_L - e_H)\, exp\left[-\left(\frac{\sigma'_z}{\sigma'_c}\right)^{\eta}\right] \tag{2}$$

where the model parameter η characterizes the sensitivity of the void ratio to effective stress, typically approximated as $\eta \approx 1/3$, while σ'_c represents the characteristic effective stress.

Fig. 7 shows the laboratory test results and exponential compaction trend lines for the four specimens with D_r = 30, 50, 70, and 90%. Table 1 summarizes the constitutive model parameters for all the cases.

Despite being limited to laboratory compaction tests with dry specimens to obtain compaction curves, this study provides valuable insights by monitoring the relative density versus depth in non-compacted soil layers. Furthermore, the relative density estimation method based on a physics-inspired and data-based approach is significant in offering data that enable the intuitive delineation of boundaries between dry and saturated conditions. Further details follow.

5.2 Soil compressibility model – Effective stress versus depth

This study used the effective stress–depth model for two extreme cases: completely (1) dry and (2) saturated conditions. In terms of the relationship between force equilibrium and the gravimetric-volumetric, the derivative of effective stress σ'_z with respect to depth can be formulated as

$$\frac{d\sigma'_z}{dz} = \frac{G_S \gamma_w}{1 + e_z} \tag{3}$$

where G_S denotes the specific gravity of dry soil. By substituting Eq. (2) into Eq. (3) and subsequently solving the resulting differential equation, the closed-form solution for $\eta \approx 1/3$ provides the effective stress profile σ'_z as a function of depth. Therefore, the effective stress profile of dry ground conditions with depth can be determined using a closed-form solution for η = 1/3 (Lyu *et al*. 2021)

$$z = \frac{(1 + e_H)}{G_S \gamma_w}\sigma'_z - 3\frac{(e_L - e_H)}{G_S \gamma_w}\sigma'_c \left\{\left[\left(\frac{\sigma'_z}{\sigma'_c}\right)^{\frac{2}{3}} + 2\left(\frac{\sigma'_z}{\sigma'_c}\right)^{\frac{1}{3}} + 2\right] \cdot exp\left[-\left(\frac{\sigma'_z}{\sigma'_c}\right)^{\frac{1}{3}}\right] - 2\right\} \tag{4}$$

In the context of saturation conditions, the effective stress gradient (i.e., $d\sigma'_z/dz$) as a function of e_z at a certain depth is expressed as follows

$$\frac{d\sigma'_z}{dz} = \gamma_w \left[\frac{G_S - 1}{1 + e_z}\right] \tag{5}$$

The effective stress profile in fully saturated ground conditions as a function of depth can be similarly calculated using a closed-form solution for $\eta \approx 1/3$

$$z = \frac{(1 + e_H)}{(G_S - 1)\gamma_w}\sigma'_z - 3\frac{(e_L - e_H)}{(G_S - 1)\gamma_w}\sigma'_c \left\{\left[\left(\frac{\sigma'_z}{\sigma'_c}\right)^{\frac{2}{3}} + 2\left(\frac{\sigma'_z}{\sigma'_c}\right)^{\frac{1}{3}} + 2\right] \cdot exp\left[-\left(\frac{\sigma'_z}{\sigma'_c}\right)^{\frac{1}{3}}\right] - 2\right\} \tag{6}$$

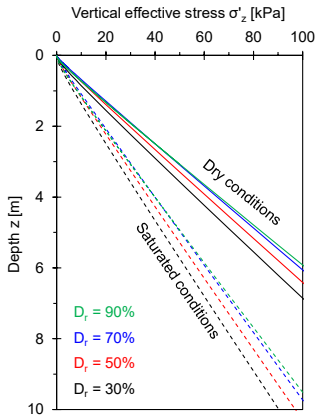

Fig. 8 Vertical effective stress-depth profiles for dry and fully saturated conditions

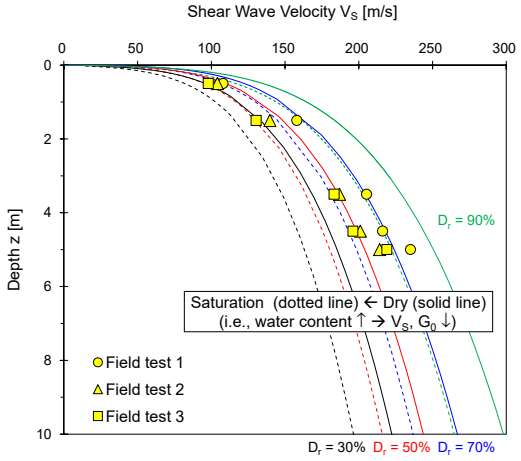

Fig. 9 Shear wave velocity-depth profiles for dry and fully saturated conditions

The profiles of effective stress versus depth are depicted for two extreme cases estimated for samples with different relative densities, as shown in Fig. 8. The results indicate that with an increase in relative density, the effective stress at equivalent depths also increases.

5.3 Estimation of relative density using shear wave velocity and Validation using DCPI

The shear wave velocity can be expressed in terms of vertical effective stress (σ'_z) at a certain depth.

$$V_S = \alpha \left(\frac{\sigma_z^{'}}{1\ \text{kPa}} \right)^{\beta} \tag{7}$$

where the αfactor represents the shear wave velocity under a stress of 1 kPa, and the βexponent indicates the sensitivity of the shear wave velocity to variations in the vertical effective stress (Santamarina *et al*. 2001). In this study, the trends in the shear wave velocity for dry specimens with different relative densities are analyzed in the context of the α-factor and β-exponent. The analytical solution and parameters of the constitutive model employed in this study provide a method to predict the effective stress σ'z with respect to depth. Consequently, by integrating the effective stress as a function of depth with the shear wave velocity as a function of the effective stress, we can anticipate a correlation between the shear wave velocity and depth. Fig. 9 shows the predicted shear wave velocity-depth profiles for completely dry and saturated conditions with different relative densities (30%, 50%, 70%, and 90%). This comparison between the shear wave velocity data and model-based trends shows that the relative density of the embankment under saturated soil conditions can vary between 50% and 90%, sometimes approaching 95%. Under dry soil conditions, the relative density of the embankment can vary from 30% to 70% and tends towards 76%.

Fig. 10 shows the changes in the void ratio-depth profiles for the two extreme cases with different relative densities (note: the e_{max} and e_{min} values of field specimen are 0.807 and 0.407, respectively). Solid lines represent dry

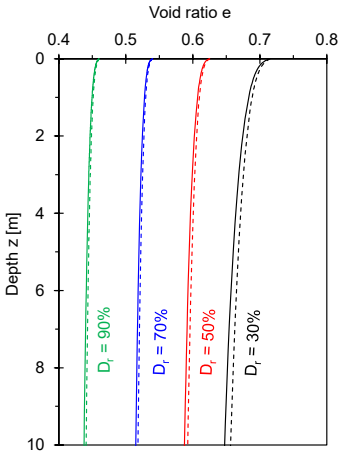

Fig. 10 Void ratio -depth profiles for dry and fully saturated conditions

conditions, whereas dotted lines denote fully saturated conditions. This trend indicates a consistent reduction in the void ratio with increasing depth across all cases, with a more pronounced decline expected in loosely compacted soil. For comprehensive analyses, void ratio-depth profiles were calculated as the relative density-depth profiles using the minimum (e_{max}) and maximum (e_{min}) compactness states (Hu *et al*. 2022)

$$D_r(\%) = \left[\frac{e_{max} - e}{e_{max} - e_{min}} \right] \times 100 \tag{8}$$

Fig. 11 plots the anticipated trends in relative density with the depth of the embankment. To validate the model, a field dynamic cone penetration test was conducted, and the relative density was computed using the empirical correlation (Mohammadi *et al*. 2008) as follows

$$D_r(\%) = \frac{189.93}{(DCPI)^{0.53}} (where R^2 = 0.98) \tag{9}$$

The relative density calculated from the DCPI data was compared with the estimated relative density–depth models

Table 2 Relative densities at each filling stage suggested by the empirical method using DCPI

Depth [m]	Relative density D_r [%]
0.5	36.0
1.5	51.7
3.5	57.1
4.5	63.3
5	77.1

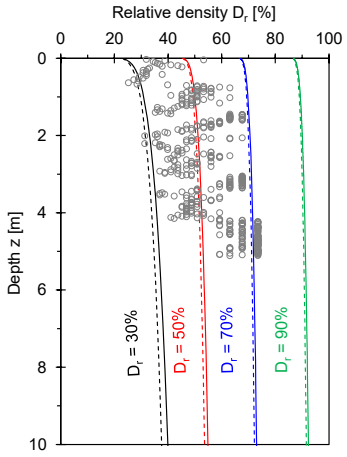

Fig. 11 Relative density-depth profiles for dry and fully saturated conditions

in the context of the void ratio (gray circles in Fig. 11). The results are averaged across depths of 0.5 m, 1.5 m, 3.5 m, 4.5 m, and 5 m, indicating relative densities of 36%, 51.7%, 57.1%, 63.3%, and 77.1%, respectively (see Table 2). Considering the dry condition of the soil in the field (i.e., in situ water content $\omega \leq 7\%$), this comparison demonstrates that the shear wave velocity successfully captures the change in the relative density of the non-compacted embankment layer.

6. Conclusions

This study introduces an embedded type in-situ soil stiffness measurement device for monitoring small strain stiffness in a non-compacted embankment layer. Comprehensive laboratory compaction tests were conducted by using an oedometer cell with a bender element. A direct comparison is extremely difficult because the shear wave velocity measured in the field and laboratory depends on the depth and effective stress, respectively. Therefore, we suggest a methodology for establishing a relationship between effective stress and depth using a compressibility model. Based on the experimental results, the following observations were made.:

- In this study, constitutive model parameters derived from laboratory test results were used to obtain a compaction curve at very low and high effective stress levels. Subsequently, the laboratory experimental results for the dry specimens with relative densities of 30%, 50%, 70%, and 90% were combined with the exponential compaction trends based on the compressibility model.
- To expand the applicability of the experimental findings, we attempted to link effective stress and depth using a compressibility model. This physics-inspired approach provides vertical effective stress-depth profiles for dry and fully saturated conditions.
- The shear wave velocity measured in the field was compared with the estimated shear wave velocity-depth profiles for completely dry and saturated conditions with different relative densities. The comparison shows that the relative density under saturated soil conditions may vary between 50% and 90% and tends to be closer to 95%. Under dry soil conditions, the relative density of the embankment varied from 30% to 70% and tended to approach 76%. For model validation, the relative density estimated from the shear wave velocity-depth profiles was compared with that estimated from the DCPI data. The proposed relationships demonstrate that this data interpretation approach successfully captures the relative density of a non-compacted embankment layer.

Acknowledgments

This work was supported by the National Research Foundation of Korea (NRF) grant funded by the Korea government (MSIT) (No. NRF-2021R1A5A1032433).

References

Andrus, R.D. and Stokoe II, K.H. (2000), "Liquefaction resistance of soils from shear-wave velocity", *J. Geotech. Geoenviron. Eng.*, **126**(11), 1015-1025. https://doi.org/10.1061/(asce)1090-0241(2000)126:11(1015)

ASTM, D. (2020), Standard test methods for one-dimensional consolidation properties of soils using incremental loading. ASTM Stand. ASTM, D2435/C2435M-11.

Brown, L.T., Boore, D.M. and Stokoe, K.H. (2002), "Comparison of shear-wave slowness profiles at 10 strong-motion sites from noninvasive SASW measurements and measurements made in boreholes", *Bull. Seismol. Soc. Am.*, **92**(8), 3116-3133. https://doi.org/10.1785/0120020030

Burland, J.B. (1990), "On the compressibility and shear strength of natural clays", *Géotechnique*, **40**(3), 329-378. https://doi.org/10.1680/geot .1990.40.3.329

Byun, Y.H., Hong, W.T. and Lee, J.S. (2015), "Characterization of railway substructure using a hybrid cone penetrometer", *Smart Struct. Syst., Int. J.*, **15**(4), 1085-1101. http://dx.doi.org/10.12989/sss.2015.15.4.1085

Chang, M.F., Yu, G., Na, Y.M. and Choa, V. (2006), "Evaluation of relative density profiles of sand fill at a reclaimed site", *Can. Geotech. J.*, **43**(9), 903-914. https://doi.org/10.1139/t06-053

Chian, S.C., Tan, B.C.V. and Sarma, A. (2017), "Reprint of: Projectile penetration into sand: Relative density of sand and projectile nose shape and mass", *Int. J. Impact Eng.*, **105**, 80-88. https://doi.org/10.1016/j.ijimpeng.2017.03.026

Choi, C., Jeong, Y.H., Baek, S.H., Kim, J.Y., Kim, N. and Cho, J.W. (2021). "A Study for Deriving Target CMV (Compaction Meter Value) of Intelligent Compaction Earthwork Quality

Control", *J. Geol. Soc. Korea*, **37**(9), 25-36. https://doi.org/10.7843/kgs.2021.37.9.25

Chong, S.H. and Santamarina, J.C. (2016), "Soil compressibility models for a wide stress range", *J. Geotech. Geoenviron. Eng.*, **142**(6), 06016003. https://doi.org/10.1061/(ASCE)GT.1943-5606.0001482

He, S.H., Ding, Z., Xia, T.D., Zhou, W.H., Gan, X.L., Chen, Y.Z. and Xia, F. (2020), "Long-term behaviour and degradation of calcareous sand under cyclic loading", *Eng. Geol.*, **276**, 105756. https://doi.org/10.1016/j.enggeo.2020.105756

Hoang, N.Q., Kim, S.Y. and Lee, J.S. (2022), "Compressibility, stiffness and electrical resistivity characteristics of sand–diatom mixtures", *Géotechnique*, **72**(12), 1068-1081. https://doi.org/10.1680/jgeot.20.P.136

Hu, W., Li, Y., Fan, Y., Xiong, M., Luo, H., McSaveney, M., Zheng, Y. and Tang, M. (2022), "Flow amplification from cascading landslide dam failures: Insights from flume experiments", *Eng. Geol.*, **297**, 106483. https://doi.org/10.1016/j.enggeo.2021.106483

Ifediniru, C. and Ekeocha, N.E. (2022), "Performance of cement-stabilized weak subgrade for highway embankment construction in Southeast Nigeria", *Int. J. Geo-Eng.*, **13**(1), 1. https://doi.org/10.1186/s40703-021-00166-z

Ji, Y., Kim, B. and Kim, K. (2021), "Evaluation of liquefaction potentials based on shear wave velocities in Pohang City, South Korea", *Int. J. Geo-Eng.*, **12**, 1-10. https://doi.org/10.1186/s40703-020-00132-1

Karimpour-Fard, M., Zarbakhash, S., Soufi, G.R., Ahadi, A. and Naveen, B.P. (2020), "Design, fabrication and calibration of a tall pneumatic oedometer apparatus", *Measurement*, **163**, 107985. https://doi.org/10.1016/j.measurement.2020.107985

Kim, D.S., Shin, M.K. and Park, H.C. (2001), "Evaluation of density in layer compaction using SASW method", *Soil Dyn. Earthq. Eng.*, **21**(1), 39-46. https://doi.org/10.1016/S0267-7261(00)00076-2

Kim, S.Y., Lee, J.S. and Hong, W.T. (2021), "Subgrade assessment using automated dynamic cone penetrometer to manage geo-infrastructures", *Smart Struct. Syst.*, *Int. J.*, **27**(5), 861-870. https://doi.org/10.12989/sss.2021.27.5.861

Kim, N., Park, G., Kim, S.Y., Lee, J.S. and Park, J. (2024), "Physics-inspired geophysical assessment of liquefaction potential in Pohang, South Korea", *Acta Geotechnica*, 1-15. https://doi.org/10.1007/s11440-023-02083-0

Lee, J.S. and Santamarina, J.C. (2005), "Bender elements: performance and signal interpretation", *J. Geotech. Geoenviron. Eng.*, **131**(9), 1063-1070. https://doi.org/10.1061/(asce)1090-0241(2005)131:9(1063)

Lyu, C., Park, J. and Carlos Santamarina, J. (2021), "Depth-dependent seabed properties: Geoacoustic assessment", *J. Geotech. Geoenviron. Eng.*, **147**(1), 04020151. https://doi.org/10.1061/(ASCE)GT.1943-5606.0002426

MacRobert, C.J., Bernstein, G.S. and Nchabeleng, M.M. (2019), "Dynamic cone penetrometer (DCP) relative density correlations for sands", *Soils Rocks*, **42**(2). https://doi.org/10.28927/SR.422201

Mohammadi, S.D., Nikoudel, M.R., Rahimi, H. and Khamehchiyan, M. (2008), "Application of the Dynamic Cone Penetrometer (DCP) for determination of the engineering parameters of sandy soils", *Eng. Geol.*, **101**(3-4), 195-203. https://doi.org/10.1016/j.enggeo.2008.05.006

Mokhtari, M., Shariatmadari, N., Heshmati R, A.A. and Salehzadeh, H. (2015), "Design and fabrication of a large-scale oedometer", *J. Cent. South Univ.*, **22**, 931-936. https://doi.org/10.1007/s11771-015-2603-x

Naing, T., Pramumijoyo, S. and Kawase, H. (2015), "Estimation of S-Wave Velocity Structures in Yogyakarta Basin, Indonesia", *J. Appl. Geol.*, **1**(2). https://doi.org/10.22146/jag.7228

NEHRP (2003), Recommended provisions for seismic regulations for new buildings and other structures, In: Building Seismic Safety Council (BSSC) for the Federal Emergency Management Agency (FEMA 450), FEMA, Washington Part 1: Provisions.

Pestana, J.M. and Whittle, A.J. (1995), "Compression model for cohesionless soils", *Géotechnique*, **45**(4), 611-631. https://doi.org/10.1680/geot.1995.45.4.611

Park, G., Kim, N., Hong, W.T. and Lee, J.S. (2022), "Rod effects on transferred energy into SPT sampler using smart measurement system", *Smart Struct. Syst.*, *Int. J.*, **30**(2), 159-172. https://doi.org/10.12989/sss.2022.30.2.159

Santamarina, J.C., Klein, A. and Fam, M.A. (2001), "Soils and waves: Particulate materials behavior, characterization and process monitoring", *J. Soils Sediments*, **1**(2), 130-130. https://doi.org/10.1007/bf02987719

Spagnoli, G. and Shimobe, S. (2020), "An overview on the compaction characteristics of soils by laboratory tests", *Eng. Geol.*, **278**, 105830. https://doi.org/10.1016/j.enggeo.2020.105830

Stewart, W.P. and Campanella, R.G. (1993), "Practical aspects of in situ measurements of material damping with the seismic cone penetration test", *Can. Geotech. J.*, **30**(2), 211-219. https://doi.org/10.1680/geot.1995.45.4.611

Terzaghi, K., Peck, R.B. and Mesri, G. (1996), *Soil Mechanics in Engineering Practice*, John wiley & sons.